THE RELATIONSHIP BETWEEN THE VERTICAL MOTION AT THE TOP OF THE FRICTION LAYER AND THE GEOSTROPIC VORTICITY AS A FUNCTION OF THE ROSSBY NUMBER

Carl Walter Hoffman

NAVAL POSTGRADUATE SCHOOL
Monterey, California

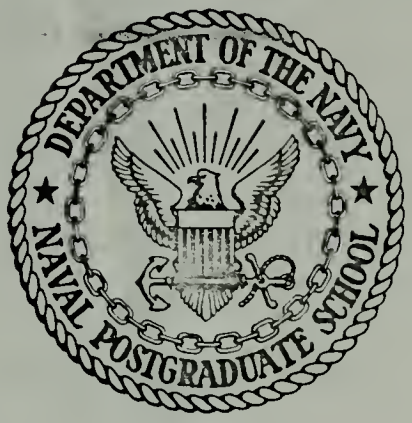

THESIS

The Relationship Between the Vertical Motion at the Top of the Friction Layer and the Geostropic Vorticity as a Function of the Rossby Number

by

Carl Walter Hoffman

Thesis Advisor: Roger T. Williams

March 1972

Approved for public release; distribution unlimited.

The Relationship Between the Vertical Motion at the Top of the Friction Layer and the Geostrophic Vorticity as a Function of the Rossby Number

by

Carl Walter Hoffman
Lieutenant Commander, United States Navy
B. S., Kent State University, 1963

Submitted in partial fulfillment of the
requirements for the degree of

MASTER OF SCIENCE IN METEOROLOGY

from the

NAVAL POSTGRADUATE SCHOOL
March 1972

ABSTRACT

The relationship between vertical motion at the top of the boundary layer, geostrophic vorticity in the boundary layer and divergence in the boundary layer are examined in this study. The equation of motion and the continuity equation are applied to a homogeneous barotropic atmosphere using a numerical model in this study. The solutions reveal that the boundary layer is stable for very large values of Ro in the case of positive vorticity and becomes unstable at Ro = 1.0 in the case of negative vorticity. A difference in behavior is found between cases of anticyclonic and cyclonic shear. The magnitude of the vertical velocity is greater and the boundary is thicker for anticyclonic than for cyclonic shear systems of equivalent strength.

TABLE OF CONTENTS

LIST OF FIGURES

LIST OF SYMBOLS

f	Coriolis parameter
ν	Eddy viscosity
u	Zonal wind component
v	North-south wind component
w	$\frac{dz}{dt}$
z	Height
t	Time
V	Velocity scale
L	Horizontal space scale
D	Ekman depth scale
X	$\frac{\partial u}{\partial x}$, divergence
Y	$\frac{\partial v}{\partial x}$, vorticity
H	Height at top of atmosphere
ϕ	$\frac{p}{\rho_o}$
S	Any scalar
Ro	Rossby number
ρ_o	Constant density
p	Pressure

ACKNOWLEDGEMENTS

The author wishes to express his deep appreciation and thanks to Dr. R. Terry Williams whose interest, counsel and recommendations were truly inspiring. I would also like to thank Dr. Kenneth L. Davidson for his assistance in preparing the manuscript for this study. An additional thank you is in order for the evening crew of the W.R. Church Computer Center for expediting the numerical calculations.

I. INTRODUCTION

The importance of boundary layer flows in the dynamics of the atmosphere is well known. If the atmosphere were a homogeneous fluid in a rotating-coordinate system, the motion would be largely geostrophic outside of the boundary layer and the velocity components would not change in a direction parallel to the axis of rotation. Thus, a substantial part of the cross-isobaric mass transport would take place in a thin layer near the earth's surface. Although the earth's atmosphere is not homogeneous, the same processes hold.

The structure of the boundary layer in a homogeneous rotating fluid was first examined by Ekman in 1905 who derived the velocity field resulting from a semi-infinite, uniform current in geostrophic equilibrium moving over a plane surface. The Ekman solution has played an important part in our effort to understand the behavior of the atmospheric fluid system. The cross-isobaric mass transport in the Ekman layer is proportional to the geostrophic speed and it has long been recognized that with horizontal variation in speed, an inevitable result will be the establishment of horizontal divergence or convergence in the boundary layer. This, in turn, leads to vertical velocities which may be of meteorological importance.

Charney and Eliassen (1949) showed that a first approximation, neglecting inertia terms, indicates that the vertical velocity at the top of the boundary layer is proportional to the relative vorticity. This result agrees with the simple picture which gives rising motion over a low from the cross-isobar flow and sinking motion over a high.

The objective of this study is to generalize the previous theory to cases where the Rossby number is not small. These results will be important for tropical motions and mesoscale motions. A study by Benton (1964) assumed steady-state flow and involved an expansion in the Rossby number. Benton's steady-state condition may not be valid and his expansion in the Rossby number will not be correct for a Rossby number greater than order one. This study was accomplished by solving the appropriate equations numerically without those approximations.

II. BASIC EQUATIONS

Numerical experiments were conducted using two one-dimensional models and one two-dimensional model. Model 1 is one-dimensional in the vertical, with the area bounded by a rigid surface at the bottom and unbounded at the top. Model 2 is also one-dimensional in the vertical and is bounded by rigid surfaces both at the top and at the bottom. Model 3 is two-dimensional in the east-west direction and in the vertical. It is also bounded by rigid surfaces at the top and at the bottom.

The equation of motion, with friction represented as:

$$\vec{F} = \nu \frac{\partial^2 \vec{V}^*}{\partial z^2} \quad ,$$

plus the continuity equation form a complete set for the calculations in all three models. If the grid area is considered homogeneous in the y direction, $\frac{\partial}{\partial y} \equiv 0$, and the atmosphere is considered a homogeneous fluid with constant density, this equation can be written in component form as

$$\frac{\partial u^*}{\partial t^*} + u^* \frac{\partial u^*}{\partial x^*} + w^* \frac{\partial u^*}{\partial z^*} = f(v^* - v_g^*) + \nu \frac{\partial^2 u^*}{\partial z^{*2}} \quad , \tag{1}$$

$$\frac{\partial v^*}{\partial t^*} + u^* \frac{\partial v^*}{\partial x^*} + w^* \frac{\partial v^*}{\partial z^*} = -f u^* + \nu \frac{\partial^2 v^*}{\partial z^{*2}} \tag{2}$$

$$\frac{\partial u^*}{\partial x^*} + \frac{\partial w^*}{\partial z^*} = 0 \tag{3}$$

Further, application of the hydrostatic equation leads to:

$$\frac{\partial \vec{V}_g^*}{\partial z^*} = 0.$$

We non-dimensionalize by choosing $t^* = \frac{1}{f}\, t$, $u^* = Vu$,

$$v_g^* = Vv_g,\ v^* = Vv,\ w^* = \frac{VD}{L}\ w,\ x^* = L\ x,\ z^* = Dz,$$

$$D = \sqrt{\frac{\gamma}{f}}\ ,\ Ro = \frac{V}{fL}$$

and apply these to equations (1), (2) and (3) which gives:

$$\frac{\partial u}{\partial t} + Ro\left[u\frac{\partial u}{\partial x} + w\frac{\partial u}{\partial z}\right] = v - v_g + \frac{\partial^2 u}{\partial z^2} \tag{4}$$

$$\frac{\partial v}{\partial t} + Ro\left[u\frac{\partial v}{\partial x} + w\frac{\partial v}{\partial z}\right] = -u + \frac{\partial^2 v}{\partial z^2} \tag{5}$$

$$\frac{\partial u}{\partial x} + \frac{\partial w}{\partial z} = 0 \tag{6}$$

Suppose that u, v and v_g are odd functions of x. Then at x = 0 we will have $u = v_g = 0$, but their first derivatives will not be zero at x = 0. Additionally, define:

$$X \equiv \frac{\partial u}{\partial x}\ ,\ Y_g \equiv \frac{\partial v_g}{\partial x}\ ,\quad Y \equiv \frac{\partial v}{\partial x}$$

and differentiate equations (4) and (5) with respect to x which gives the non-dimensional form of the divergence and vorticity equations:

$$\frac{\partial X}{\partial t} + Ro\left[X^2 + w\frac{\partial X}{\partial z}\right] = Y - Y_g + \frac{\partial^2 X}{\partial z^2} \tag{7}$$

$$\frac{\partial Y}{\partial t} + Ro\left[XY + w\frac{\partial Y}{\partial z}\right] = -X + \frac{\partial^2 Y}{\partial z^2} \tag{8}$$

If we use the above definitions, the continuity equation takes the form:

$$X = -\frac{\partial w}{\partial z} \tag{9}$$

Now we apply the product rule for differentiation and equation (9) to the quantities within the brackets of equation (7) and (8) to obtain:

$$\frac{\partial X}{\partial t} + Ro\left[2X^2 + \frac{\partial (wX)}{\partial z}\right] = Y - Y_g + \frac{\partial^2 X}{\partial z^2} \tag{10}$$

$$\frac{\partial Y}{\partial t} + Ro\left[2XY + \frac{\partial (wY)}{\partial z}\right] = -X + \frac{\partial^2 Y}{\partial z^2} \tag{11}$$

A. ONE-DIMENSIONAL MODELS

In model 1 the area is bounded by a rigid horizontal plane which allows no slip at the bottom and is unbounded with no stress at the top. Since this atmosphere is very deep, it follows that Y_g takes the limiting value of Y as z gets very large. To achieve these results equations (9), (10) and (11) were solved numerically subject to the following boundary conditions:

$$X(0, t) = Y(0, t) = w(0, t) = 0 \tag{12}$$

$$\frac{\partial X}{\partial z}(H,t) = \frac{\partial Y}{\partial z}(H,t) = 0. \tag{13}$$

In model 2 the lower boundary conditions of model 1 are retained. However, an additional horizontal plane is imposed at z = H and the no stress condition is maintained at this level. Thus, the boundary conditions demand that w = 0 at both the top and the bottom of the area. The remainder of the boundary conditions are the same as given in equations (12) and (13).

Consider equation (9) integrated in the vertical with these boundary conditions imposed:

$$(w)_H - (w)_0 = -\int_0^H X\, dz = 0. \tag{14}$$

Define the vertical average:

$$(\overline{\ }) \equiv \frac{1}{H} \int ( ) \, dz \ .$$

If we use our notation, equation (14) demands that $\overline{X} = 0$ in this model. Utilizing this condition, we average equation (1) in the vertical:

$$2Ro \ \overline{X^2} = \overline{Y} - \overline{Y}_g + \overline{\left(\frac{\partial^2 X}{\partial z^2}\right)} \ , \tag{15}$$

solve for $\overline{Y}_g$ and apply the derivative boundary conditions to the third term on the right-hand side, which gives:

$$\overline{Y}_g = - 2Ro \ \overline{X^2} + \overline{Y} - \frac{1}{H} \left(\frac{\partial X}{\partial z}\right)_{z = 0.} \tag{16}$$

Since:

$$\frac{\partial v_g}{\partial z} = 0 \ ,$$

it is clear that $\overline{Y}_g = Y_g$ and the latter can be replaced in equation (10) from (16). It is interesting to note at this point that as H approaches infinity $\overline{Y}_g$ approaches the value of $\overline{Y}$. To see this, one must realize that the largest contribution to $\overline{X^2}$ occurs in the friction layer and as H gets large this layer comprises a very small percentage of the total depth.

B. TWO-DIMENSIONAL MODEL

Model 3 was formulated using the Boussinesq approximation to the equation of motion. If the variables are allowed to vary only in the x and z directions and are scaled in a manner exactly analagous to that applied to equations (1) and (2), the equation combined with the continuity equation can be written in its non-dimensional component

form as:

$$\frac{\partial u}{\partial t} + Ro\left[\frac{\partial(uu)}{\partial x} + \frac{\partial(wu)}{\partial z}\right] + \frac{\partial \phi}{\partial x} - f v = \frac{\partial^2 u}{\partial z^2} \qquad (17)$$

$$\frac{\partial v}{\partial t} + Ro\left[\frac{\partial(uv)}{\partial x} + \frac{\partial(wv)}{\partial z}\right] + u = \frac{\partial^2 v}{\partial z^2} \quad . \qquad (18)$$

The boundary conditions for this model are the same as for model 2 with the addition that all variables are cyclic in the x direction.

We consider equation (6) integrated in the vertical with the boundary conditions imposed:

$$(w)_H - (w)_0 = -\int_0^H \frac{\partial u}{\partial x}\, dz = 0 \; . \qquad (19)$$

If we use the previously defined notation, equation (19) demands that $\overline{\frac{\partial u}{\partial x}} = 0$ in this model. This equation states that $\bar{u}$ is independent of x. If the variables have proper symmetry, it follows that $\bar{u}$ must be an odd function of x which leads to $\bar{u} = 0$. Again, we satisfy the constraints of the boundary conditions by averaging the u component equation in the vertical and solving for $\overline{\frac{\partial \phi}{\partial x}}$:

$$\overline{\frac{\partial \phi}{\partial x}} = \overline{\frac{\partial(uu)}{\partial x}} + \bar{v} + \frac{1}{H}\left[\frac{\partial u}{\partial z}\right]_{z=0} \; . \qquad (20)$$

We can substitute this directly into equation (17) since our model atmosphere has constant density and:

$$\overline{\frac{\partial \phi}{\partial x}} = \frac{\partial \phi}{\partial x} \; .$$

III. FINITE-DIFFERENCE APPROXIMATIONS

Equations (9), (10), (11), (6), (17) and (18) are solved numerically by introducing finite-differences in x, z and t. All solutions are obtained by a simple time marching process. The vertical domain is divided into K layers of equal thickness and the surfaces separating the layers are denoted by k. The arrangement of variables is shown in Figure 1. The vertical grid structure was introduced by Lorenz (1960) for use in the balance equations.

In this grid system the finite-difference approximation to the divergence of the vertical flux of the scalar S at $z = z_k$ is approximated by:

$$\left[\frac{\partial(wS)}{\partial z}\right]_k = \frac{w_{k+1}\,(S_{k+2} + S_k) - w_{k-1}\,(S_k + S_{k-2})}{2\Delta z} \tag{21}$$

In this equation, k is the grid index in the vertical and Δz is the grid length between successive S-bearing levels.

The dependent variables occur at each x grid point. The horizontal derivatives are approximated by:

$$\left(\frac{\partial S}{\partial x}\right)_i = \frac{S_{i+1} - S_{i-1}}{2\Delta x} \tag{22}$$

$$\left(\frac{\partial(uS)}{\partial x}\right)_i = \frac{(u_{i+1} + u_i)\,(S_{i+1} + S_i) - (u_i + u_{i-1})\,(S_i + S_{i-1})}{4\Delta x} \tag{23}$$

In these equations, i denotes the grid index and Δx the grid length between adjacent horizontal grid points. This is a variant of the finite-difference scheme that Arakawa (1966) developed to avoid nonlinear computational instability.

The difference equation proposed by Dufort and Frankel (1953) was used to numerically approximate the diffusion term. In our staggered grid system the difference approximation is:

$$\left[\frac{\partial^2 S}{\partial z^2}\right]_k = \frac{S_{k+2}^n - S_k^{n+1} - S_k^{n-1} + S_{k-2}^n}{\Delta z^2} \tag{24}$$

In the above equation k denotes the grid index, n the time index and Δz the interval between successive S-bearing levels. At the boundaries, normal second order differencing methods were used in conjunction with the Dufort and Frankel approximation:

$$S_k^n \simeq \frac{1}{2}\left(S_k^{n+1} + S_k^{n-1}\right) . \tag{25}$$

The finite-difference approximations of the integrals of equations (9) and (6) are:

$$w_k = -\sum_{k=1}^{K} X\Delta z \tag{26}$$

and

$$w_k = -\sum_{k=1}^{K}\left[\left(\frac{\partial u}{\partial x}\right)\Delta z\right] . \tag{27}$$

Centered time differences are used throughout the calculations with the exception of the first time step which is forward.

IV. RESULTS

In model 1 it is expected that the numerical solution should closely approximate the analytical solution to the Ekman spiral when the Rossby number (Ro) is zero. The solution at time 0 with the u-component of flow replaced by divergence, X, and the v-component replaced by vorticity, Y, is:

$$X\,(z,0) = -\sin\left(\frac{z}{\sqrt{2}}\right) e^{-\frac{z}{\sqrt{2}}} \tag{28}$$

$$Y\,(z,0) = 1 - \cos\left(\frac{z}{\sqrt{2}}\right) e^{-\frac{z}{\sqrt{2}}} \tag{29}$$

These expressions are used as initial conditions for model 1. Y_g in equation (10) takes on the limiting value of Y which is 1.

Figures 2, 3 and 4 are graphs of vertical motion at the top of model 1 with respect to time. Figure 2 shows that for Ro = 0.0 the initial conditions used in the model are the exact solutions. Figures 3 and 4 show that for Ro = 0.5 and 1.0 respectively, the initial conditions are not the exact solutions and a damped oscillation with the inertial period is excited.

Benton, Lipps and Tuann (1964) solved the Navier-Stokes equation by means of a series expansion in the Rossby number. Their non-dimensional third order solution for vertical motion at the top of the friction layer as a function of the Rossby number is:

$$w = .707\left[1 - \frac{7}{20}\,Ro + \frac{15}{160}\,Ro^2\right] .$$

Figure 5 is a graph of Benton's solution (dashed line) and our numerical solution (solid line) at the top of the region versus Rossby number.

Note that the two solutions are coincident as long as the Rossby number is one or less. The marked departure of the numerical solution from the analytical solution is induced by the upper boundary condition used in model 1 and by the failure of the model to reach a steady-state solution with the maximum vertical motion at the top for values of Ro greater than 1.0. Benton's analytical solution assumed an infinitely deep steady-state atmosphere. The initial attempt with model 1 was to simulate Benton's conditions by using an atmosphere ten times deeper than the boundary layer. However, the solution at Ro = 1.0 was corrected toward Benton's solution by increasing the depth of the atmosphere to twenty times that of the boundary layer.

Figure 6 is a graph of the variation of divergence with height for model 1. It shows that convergence is concentrated in the boundary layer and that the depth of the convergent layer decreases with increasing Rossby number. The vertical profile of vorticity in this model is essentially the same as in model 2 and is shown as figure 14.

Figure 7 is a graph of the variation of vertical motion with height for model 1 and is also an additional view of the vertical motion as a function of Rossby number. The figure shows clearly that boundary layer thickness increases as the Rossby number decreases.

Model 1 was also run using negative vorticity. In this case the limiting value of Y is -1 and Y_g changes accordingly. The initial conditions, equations (28) and (29), change correspondingly. The results are shown as figure 8 which is a graph of vertical motion at the top of

model 1 (solid line) versus Rossby number and Benton's solution (dashed line) in the case of negative vorticity. Again, the numerical solution is coincident with Benton's solution until Ro reaches 1. The departure of the numerical from the analytical solution occurs in this case because the equations used in the model incur inertial instability for values of Ro > 1.0 (Houghton, Young (1970)). This can be shown by linearizing equations (10) and (11) with $Y = Y_g + Y'$, $X = X'$ and solving the resulting differential equation for X'. Figure 9 is a graph of vertical motion versus height for model 1 in the case of negative vorticity. It shows that the boundary layer increases in thickness as the Rossby number increases in size. Comparing figures 7 and 9 also shows that the magnitude of the vertical velocity is greater for the negative vorticity case than for the positive vorticity case for a given Ro other than zero.

The initial conditions used in model 2 reflect a homogeneous atmosphere with the vertical average of the divergence equal to zero

$$X(z,0) = 0$$

$$Y(z,0) = 1 .$$

The sign of the initial condition in Y determines the sign of the vorticity in this model.

Figure 10 is a graph of the vertical motion at z = 3.4 versus time with Ro = 1.0 in model 2. Note the manifestation of the inertial period at time ≈ 6 and the exponential damping of magnitude with time. This damping is expected since the model has convergence or divergence in the upper region. This can be shown by linearizing the barotropic vorticity equation, integrating it in the vertical from the top of the boundary layer to the top of the atmosphere and solving the resulting differential equation for Y.

Figure 11 is a graph of the vertical motion at z = 3.4 and time = 6 versus Ro with vorticity positive in model 2. In this case the boundary remains stable when values of Ro as high as 10.0 are used.

Figure 12 is a graph of the vertical motion at z = 3.4 and time = 6 versus Ro with vorticity negative in model 2. The increased slope in the region of Ro = 1.0 is caused by the inertial instability incurred in this case.

Figures 13, 14 and 15 are graphs of divergence, vorticity and vertical motion, respectively, versus height at time = 6 for model 2 with Ro = 1.0. Figure 13 shows convergence concentrated in the friction layer with compensating divergence in the upper region. Figure 14 shows the absorption of vorticity in the friction layer. Figure 15 shows the vertical motion profile consistent with strong low level convergence underneath compensating divergence in the upper region.

Model 3 utilizes initial conditions which satisfy the boundary constraint in u and give a symmetric wave in v:

$$u\,(x,z,0) = 0$$

$$v\,(x,z,0) = -\sin x,\ (0 \leq x \leq 2\pi).$$

In this model the sign of the vorticity will vary in different portions of the wave. No vertical profiles extracted from model 3 are shown because the vertical profiles of divergence, vorticity and vertical motion at the symmetry points are the same as in model 2.

Figures 16 and 18 are graphs of the u-component of the wind field within the boundary layer at z = 1.05 and time = 6 for model 3 with Ro = 1.0 and 1.5 respectively. These graphs also provide the horizontal divergence with its intensity proportional to the slope of the curves.

Figures 17 and 19 are graphs of the v-component of the wind field within the boundary layer at z = 1.05 and time = 6 for model 3 with Ro = 1.0 and 1.5 respectively. These graphs also provide the horizontal vorticity with its intensity proportional to the slope of the curves.

Figures 16 and 18 show that the area between x ≈ 1.2 and x ≈ 5.2 is covered by convergence and the remainder of the area is covered by divergence. Figures 17 and 19 show that the convergent area contains positive vorticity and the divergent area contains negative vorticity. Since the net effect of vertical motion must be compensating, it follows that the subsidence over the narrower divergent, negative vorticity areas must be more intense than the upward vertical motion over the wider convergent, positive vorticity areas. Benton, Lipps and Tuann (1964) also found that in cases of anticyclonic shear the magnitude of the vertical velocity is greater than that for cyclonic shear systems of equivalent strength. Though a graph is not shown, inspection of the output of model 3 reveals that the boundary layer is shallower over the convergent area where the vorticity is positive than over the divergent area where the vorticity is negative.

Figures 18 and 19 show that for the case of Ro = 1.5 the solutions are smooth in the regions of positive vorticity and continue the same pattern as in the Ro = 1.0 case. That is, the solutions have a wide region of surface convergence and a narrow region of surface divergence. However, we encounter inertial instability, as predicted earlier, in the region where vorticity is negative. The instability is shown by the small-scale oscillations in the graphs.

V. CONCLUSIONS

We have constructed one and two-dimensional models with and without constraints on the vertical motion at the top of the atmosphere. The models have enabled us to make a detailed determination of the boundary layer structure as a function of the Rossby number. Benton, Lipps, and Tuann (1964) carried out a similar investigation with linear steady-state velocity fields and computed solutions using a series expansion in the Rossby number. We compared their solution for w at the top of an unbounded atmosphere with our model 1. We could not compute vertical motions to compare with their solution beyond Ro = 1.0 because the model incurred upper boundary problems in that region. In both of these studies, however, w was found to decrease in magnitude with increasing Rossby number in the case of positive vorticity. In addition, the numerical solutions show the boundary layer thickness decreasing with increasing Rossby number in the case of positive vorticity and increasing with increasing Rossby number in the case of negative vorticity.

The graph of vertical motion versus Rossby number produced from model 2 is smooth for values of Ro up to 10.0 showing that the boundary layer is stable in the region of Ro = 1.0. The vertical motion computed using model 2, however, is not suitable for comparison because its boundary conditions lead to a finite divergence or convergence in the upper region which prevents it from reaching a non-zero steady-state.

The two-dimensional model was introduced to determine the spatial structure of the boundary layer when the upper level flow is sinusoidal. Its vertical motion at the symmetry points was compared to the vertical motion of model 2 as a check since both models have consistent boundary

conditions. Analysis shows the patterns produced in the various parts of the wave are consistent with the one-dimensional analysis. That is, small vertical motions and small boundary layer thickness are found in the troughs and larger vertical motions and larger boundary layer thickness are found in the ridges. When the model was run with the Rossby number larger than 1.0, inertial instability was encountered in the ridge areas as predicted by models 1 and 2.

The models have yielded information about the boundary layer in the tropics where the Rossby number is not small. In the case of cyclonic flow, the boundary layer remains stable up through Rossby numbers of 10.0. In the case of anticyclonic flow, inertial instability renders the boundary layer unstable for Rossby numbers greater than 1.0 (Houghton, Young (1970)). The effects of the Rossby number varying with time, such as would be encountered for a moving wave case (Holton, Wallace, Young (1971)), were not considered.

Further studies should be made using a non-laminar boundary layer diffusion coefficient which changes with height and is related to the friction velocity. In particular, the depth of the boundary layer will be proportional to the friction velocity divided by f. The effect of stability near the surface and through the layer should be considered with the same model.

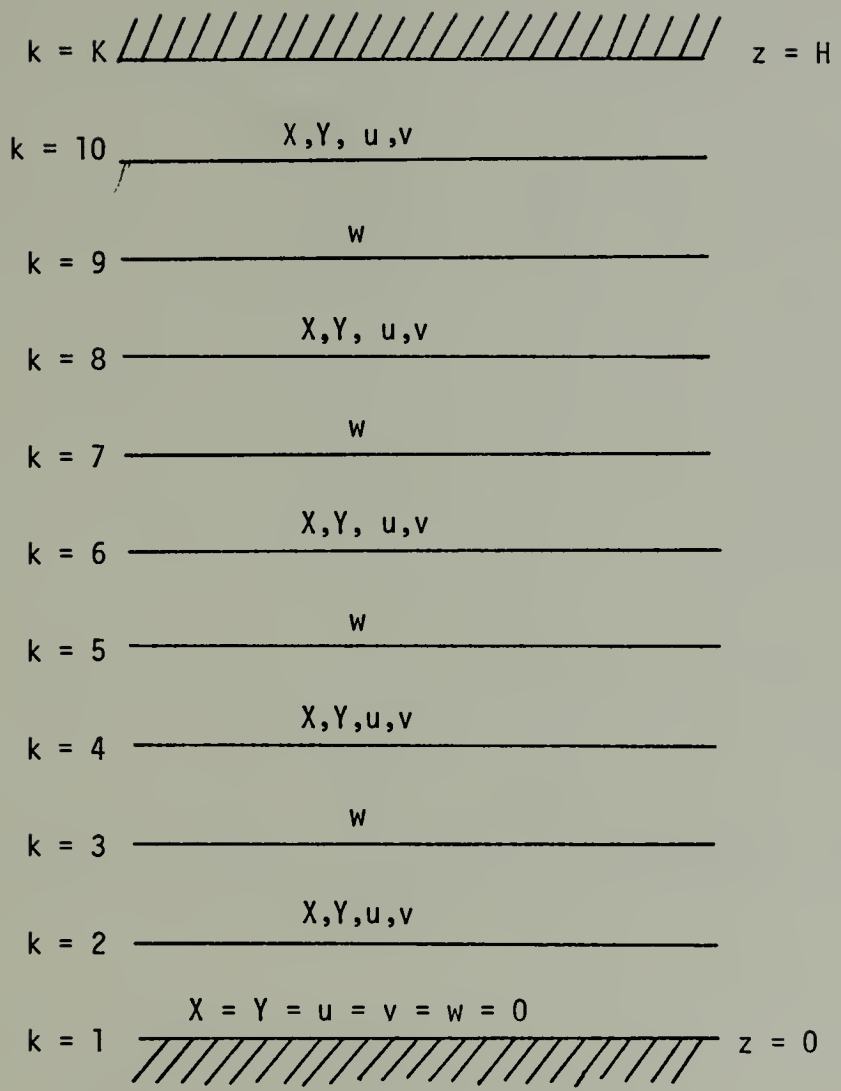

Figure 1. Arrangement of Variables in the Vertical.

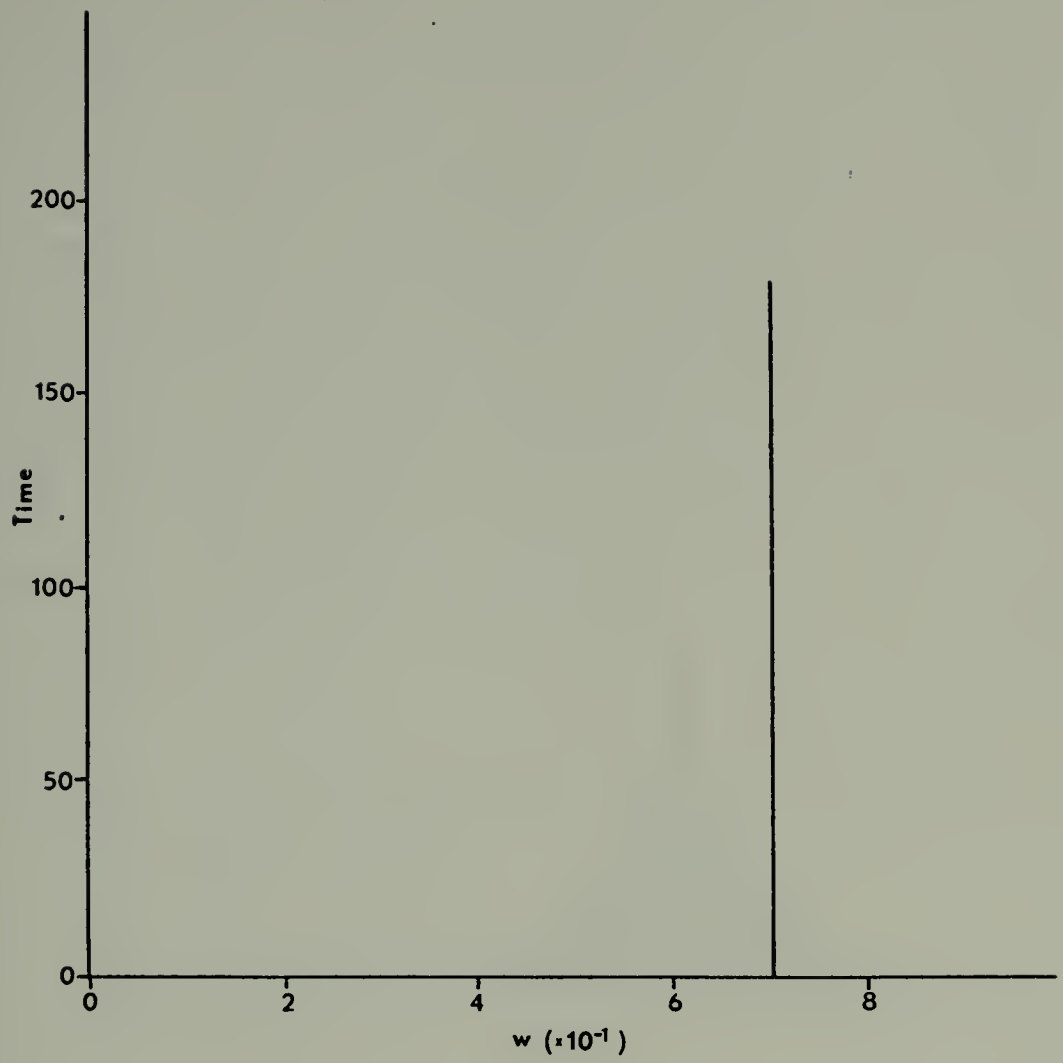

Figure 2. Variation of Vertical Motion at the Top of Model 1 with Time for Ro = 0.0, Y_g = 1.

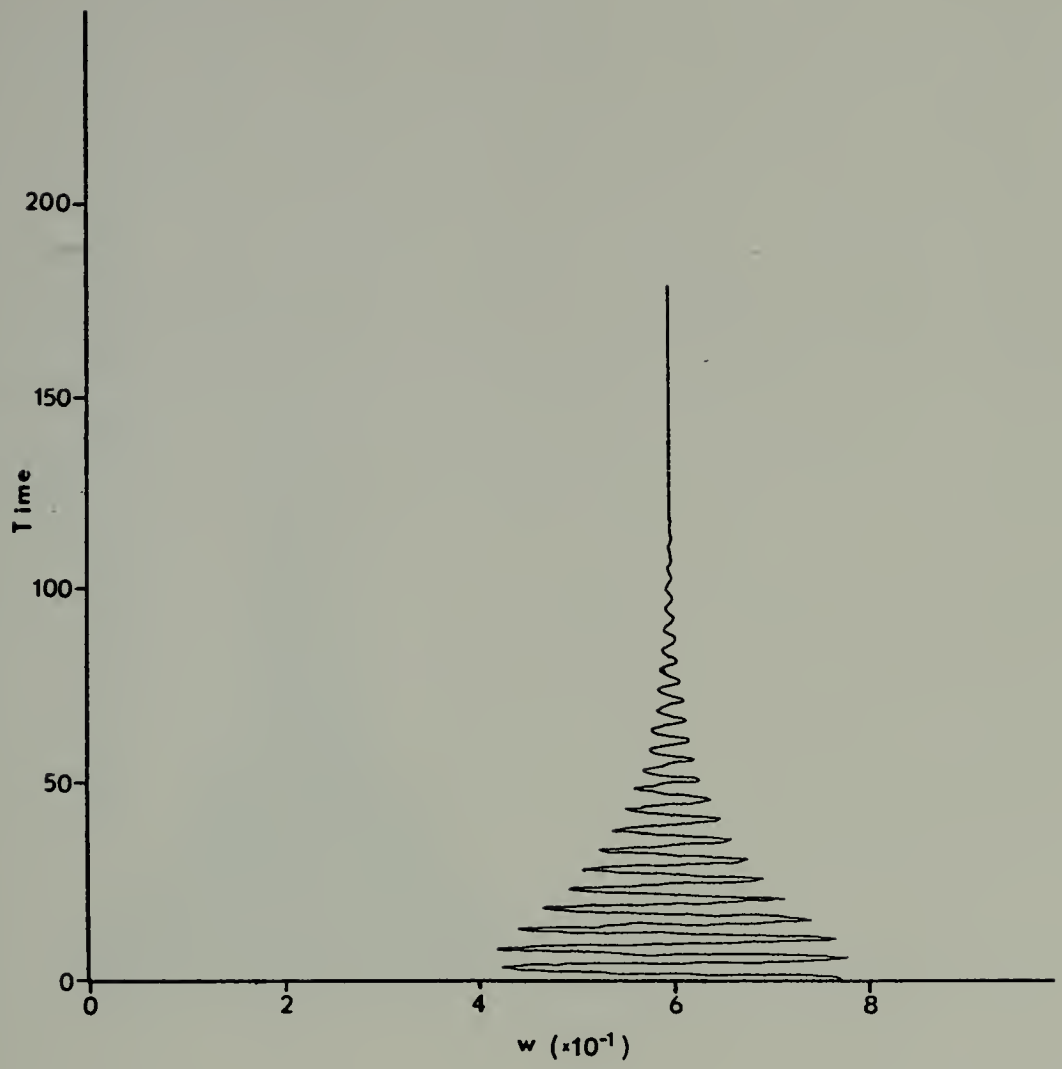

Figure 3. Variation of Vertical Motion at the Top of Model 1 with Time for Ro = 0.5, Y_g = 1.

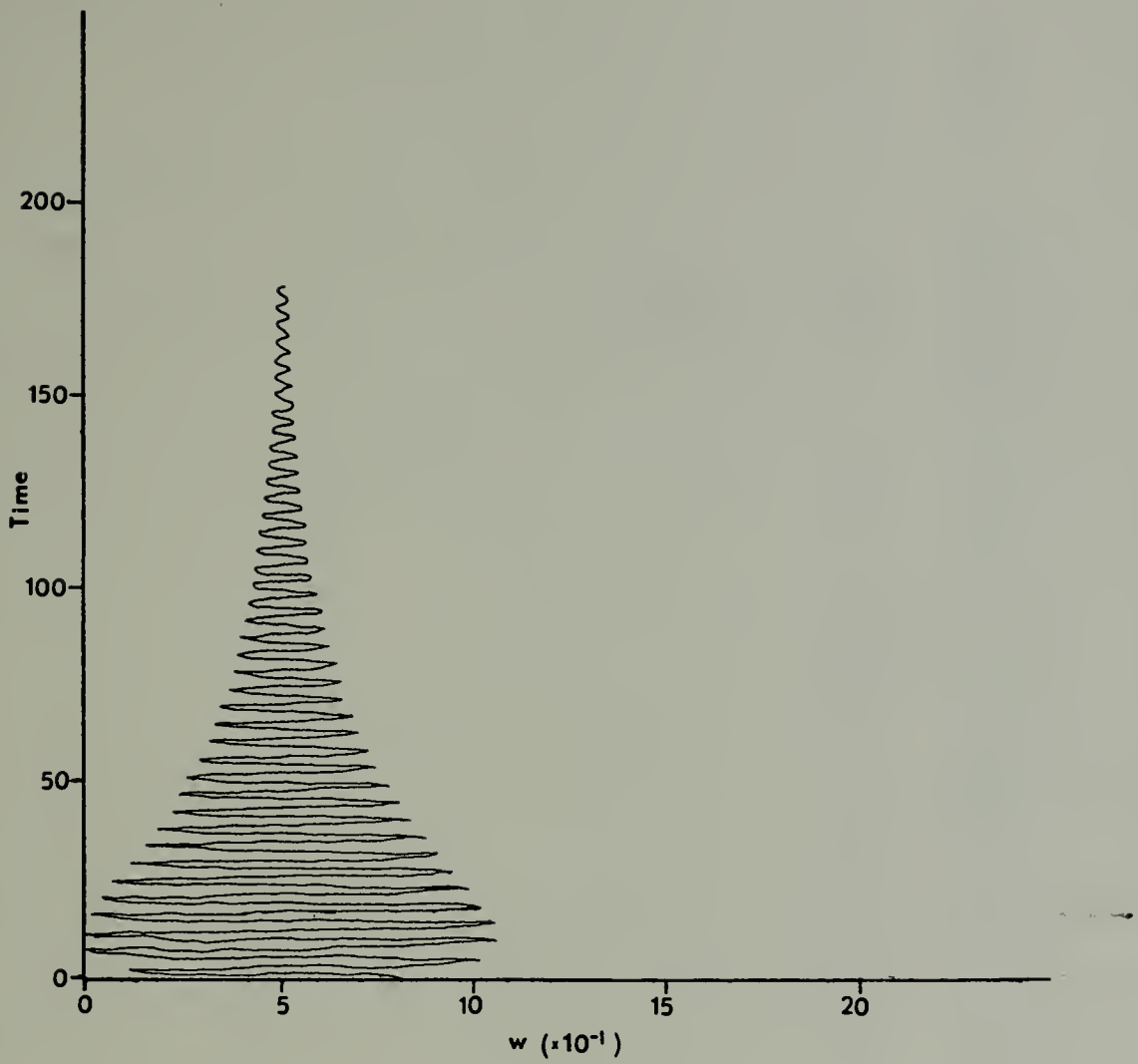

Figure 4. Variation of Vertical Motion at the Top of Model 1 with Time for Ro = 1.0, Y_g = 1.

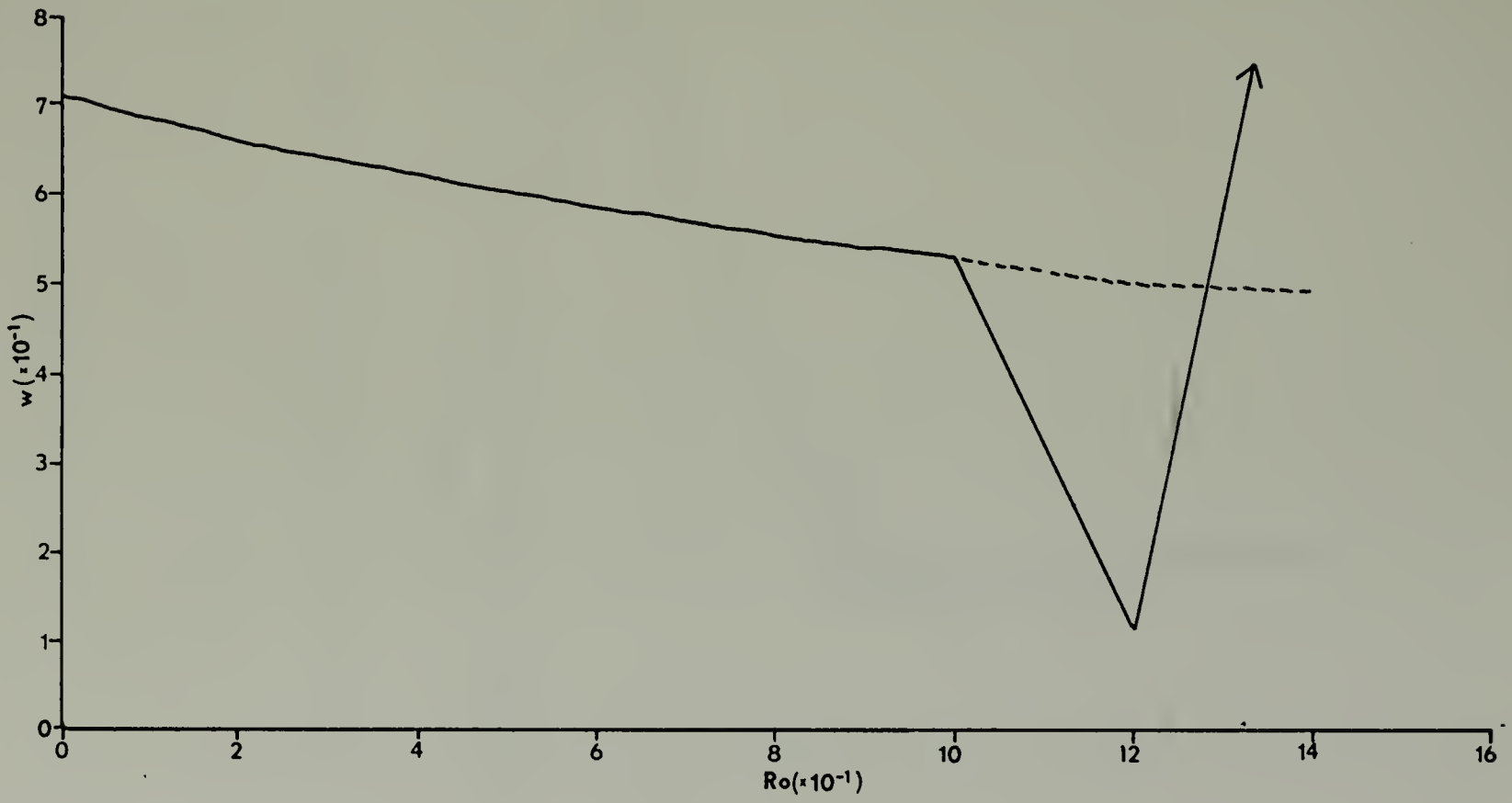

Figure 5. Variation of Vertical Motion at z = 10 (solid line) for Y_g = 1 in Model 1 and Benton's Solution (dashed line) versus Rossby Number.

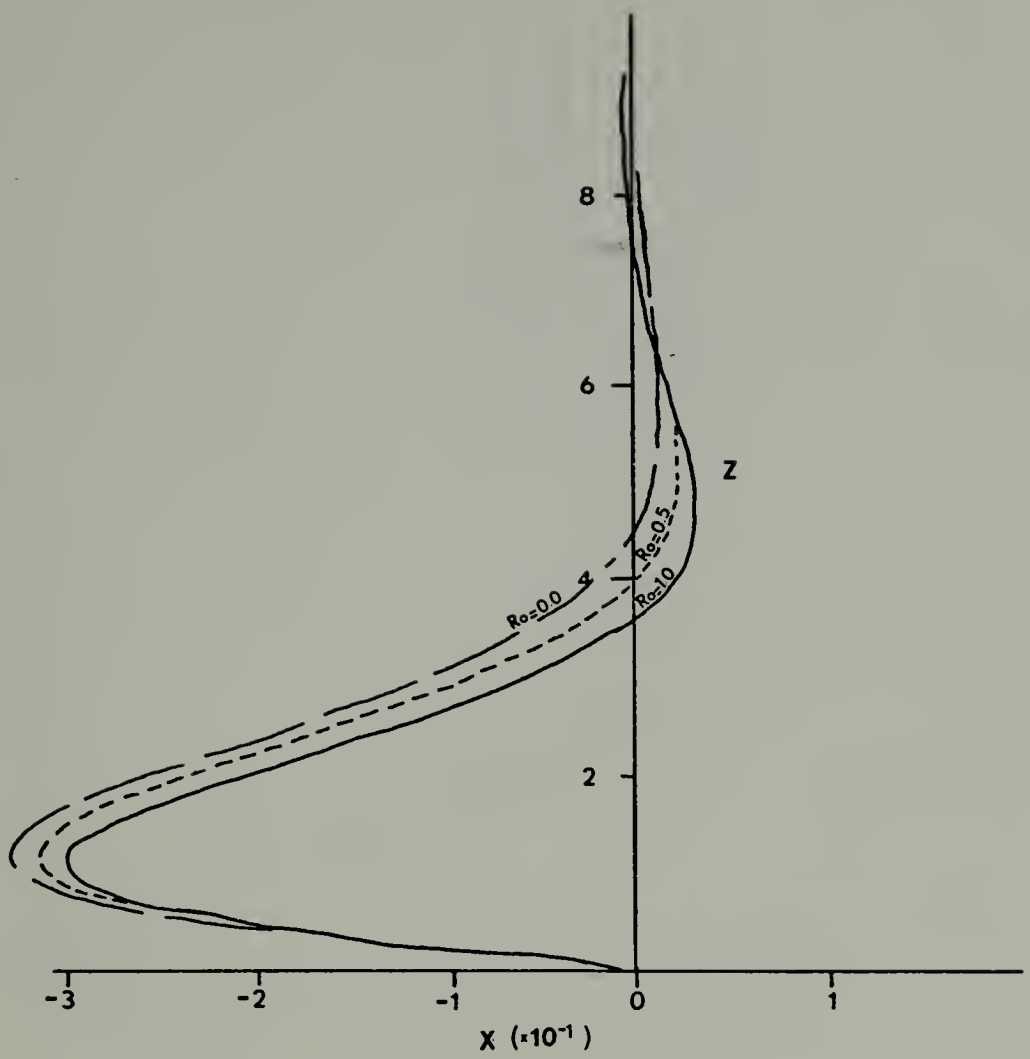

Figure 6. Variation of Divergence with Height for Model 1, Y_g = 1.

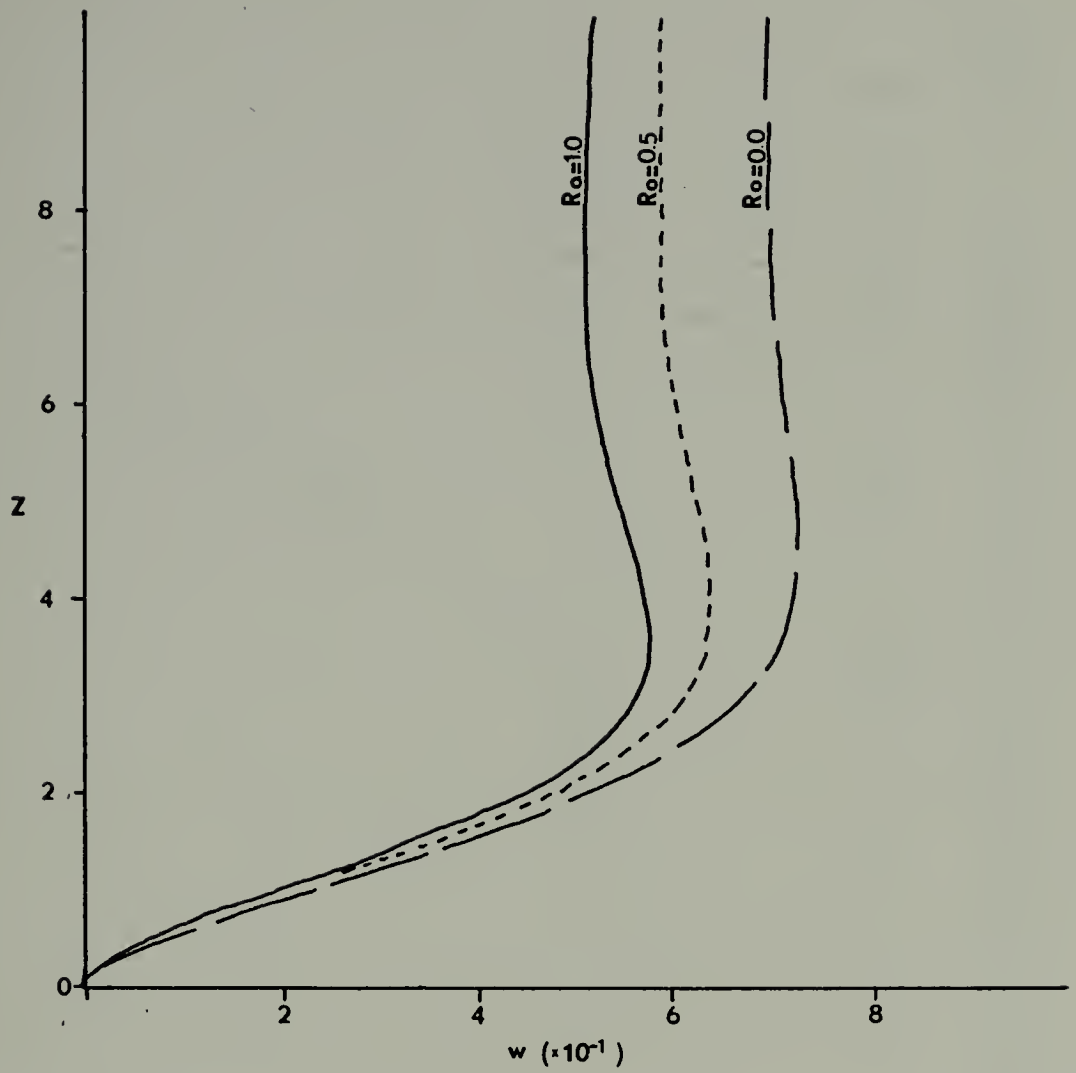

Figure 7. Variation of Vertical Motion with Height for Model 1, $Y_g = 1$.

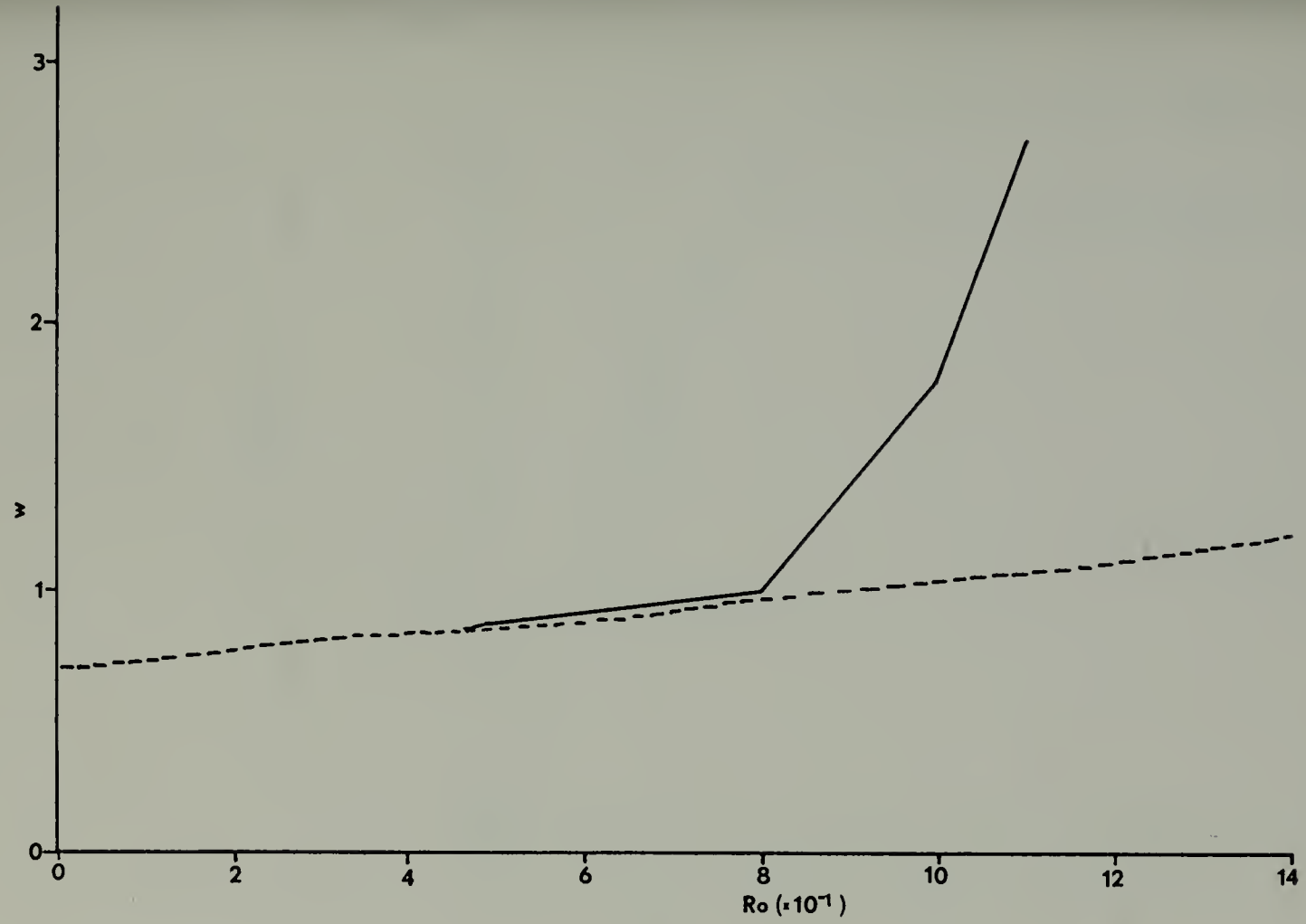

Figure 8. Variation of Vertical Motion at z = 10 (solid line) for Y_g = -1 in Model 1 and Benton's solution (dashed line) versus Rossby number.

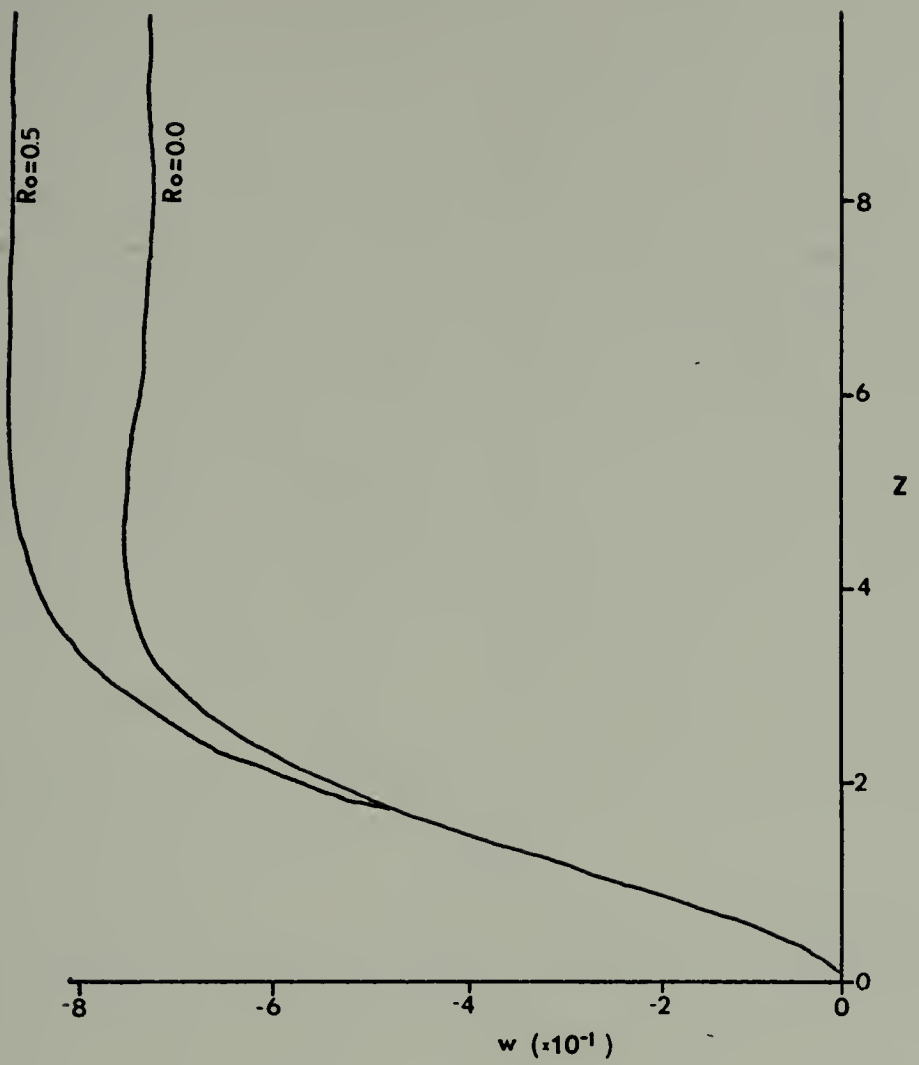

Figure 9. Variation of Vertical Motion with Height for Model 1, Y_g = -1.

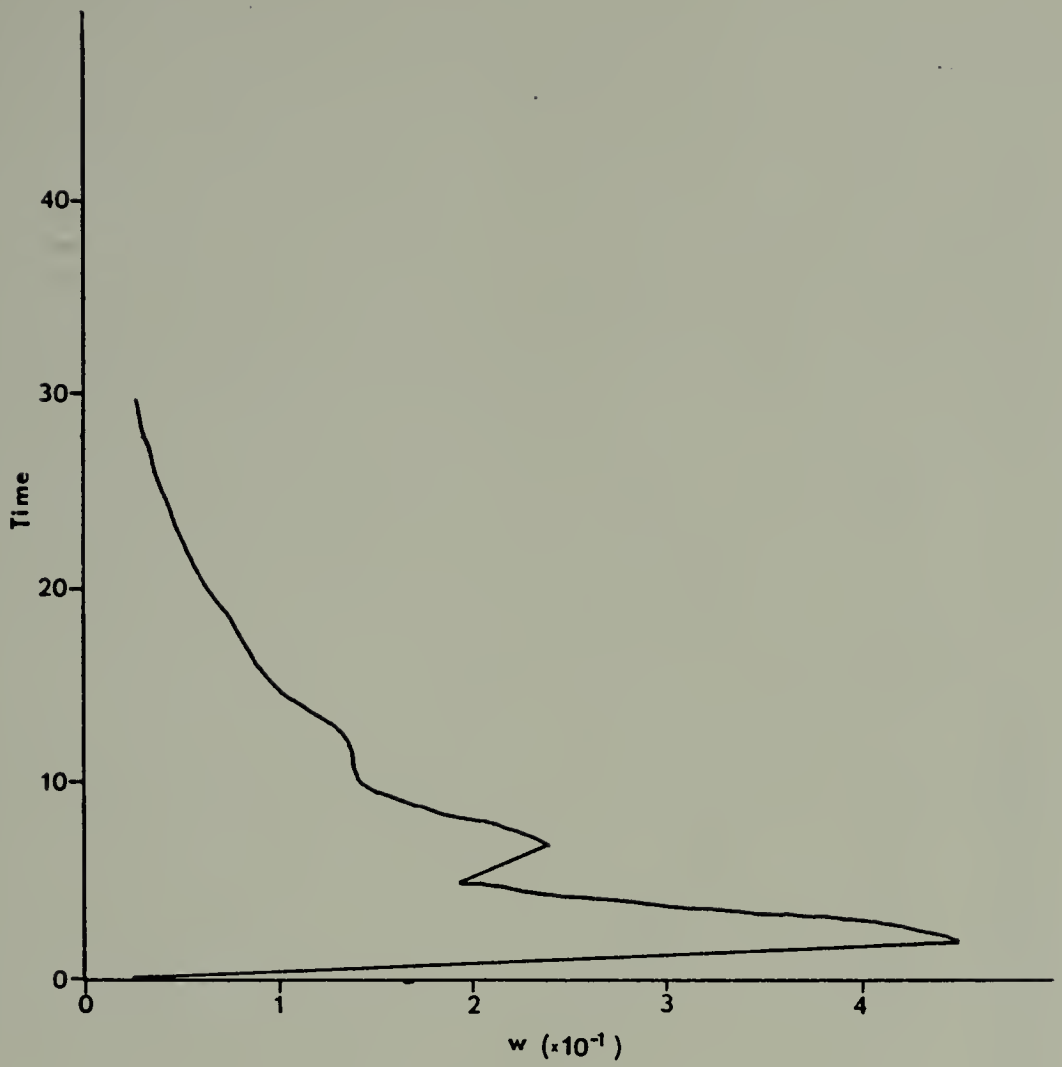

Figure 10. Variation of Vertical Motion at z = 3.4 with Time for Model 2, Ro = 1.0.

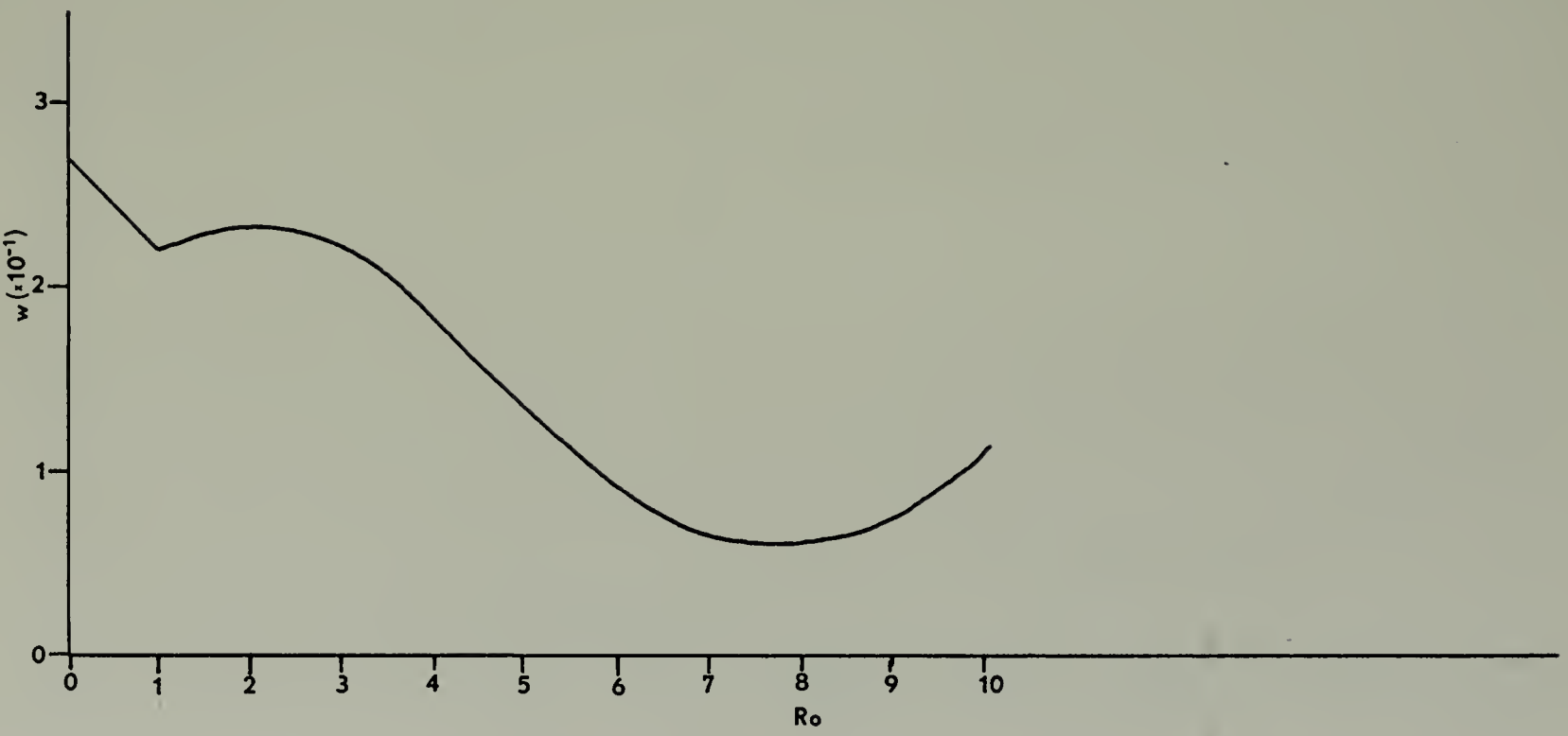

Figure 11. Variation of Vertical Motion at z = 3.4 and Time = 6 with Ro in Model 2, Vorticity Positive.

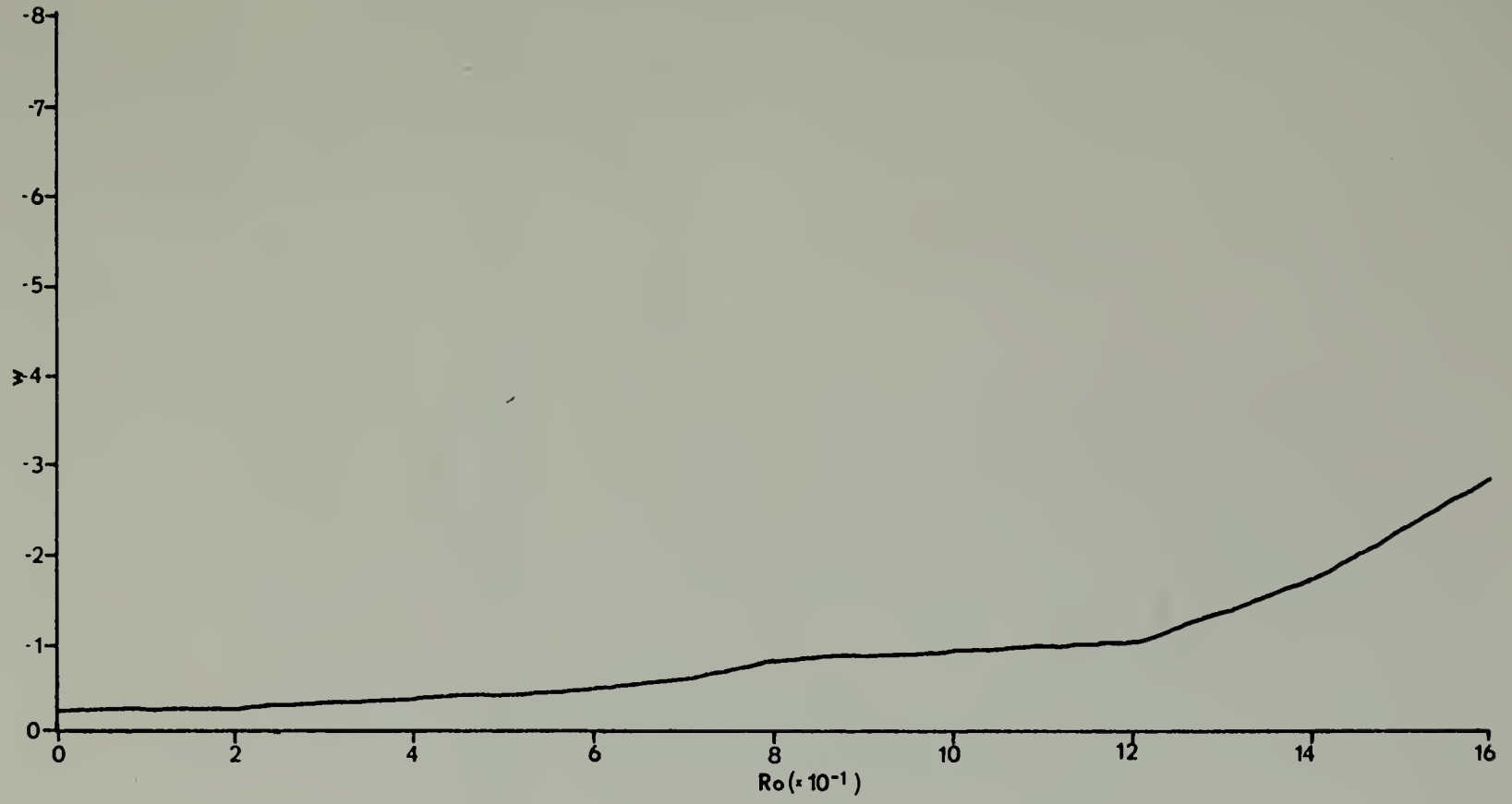

Figure 12. Variation of Vertical Motion at z = 3.4 and Time = 6 with Ro in Model 2, Vorticity Negative.

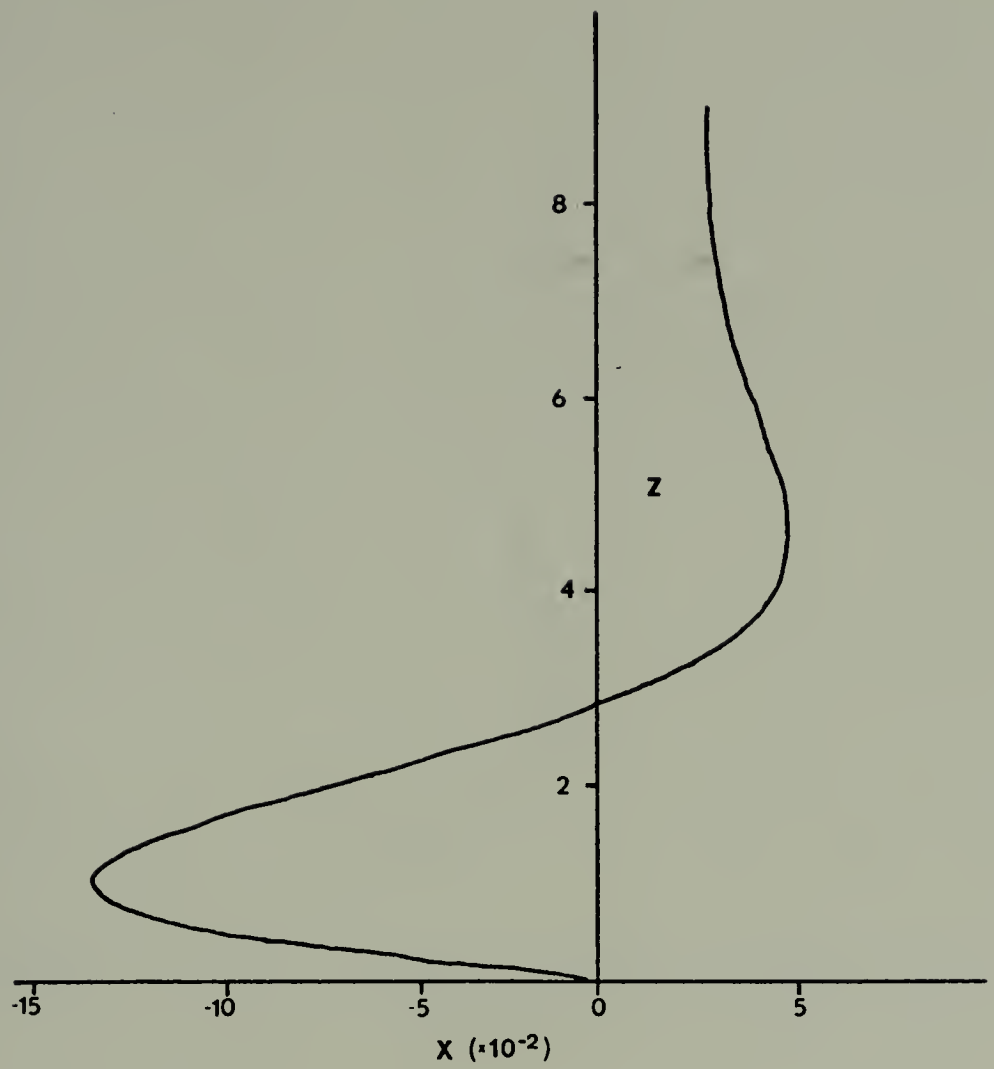

Figure 13. Variation of Divergence with Height at Time = 6 for model 2, Ro = 1.0.

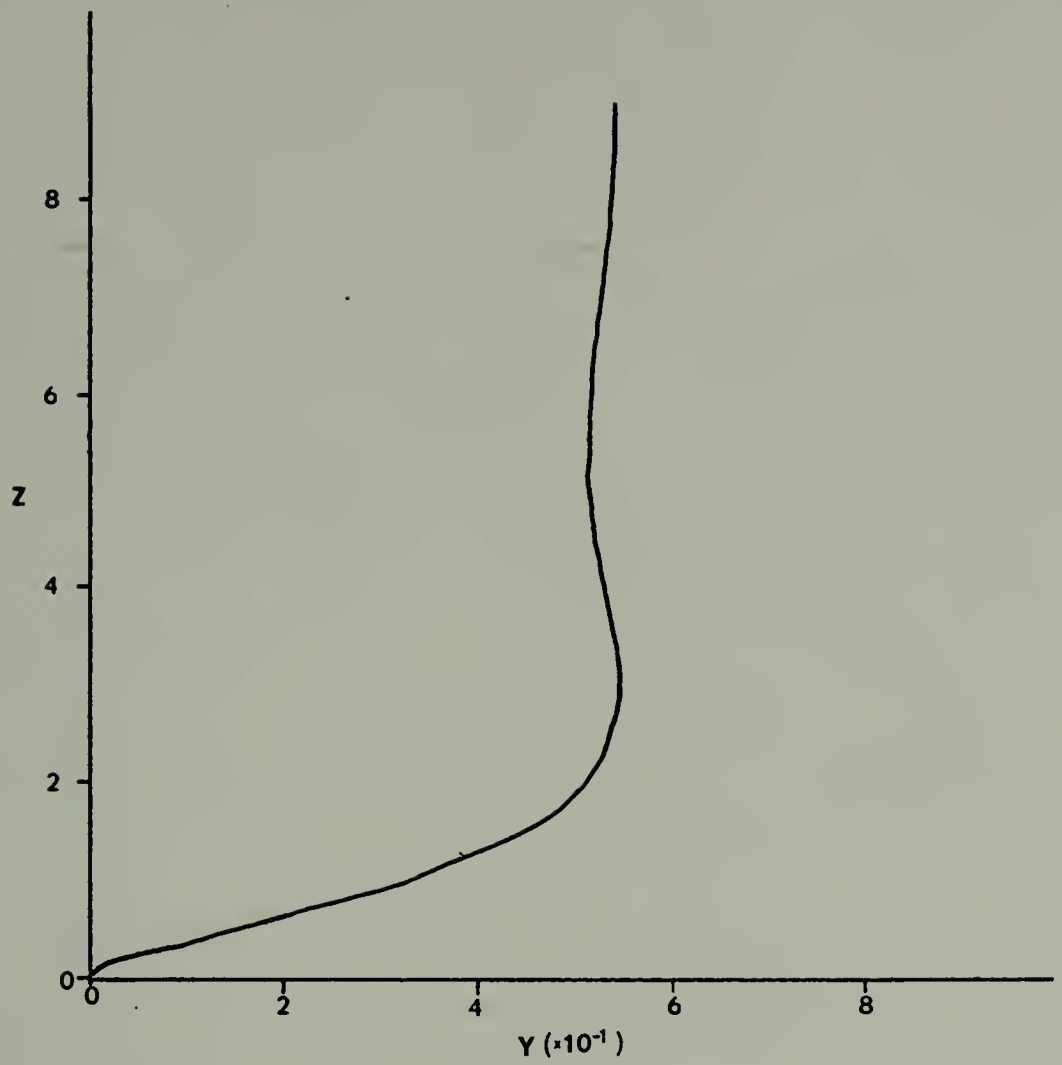

Figure 14. Variation of Vorticity with Height at Time = 6 for Model 2, Ro = 1.0.

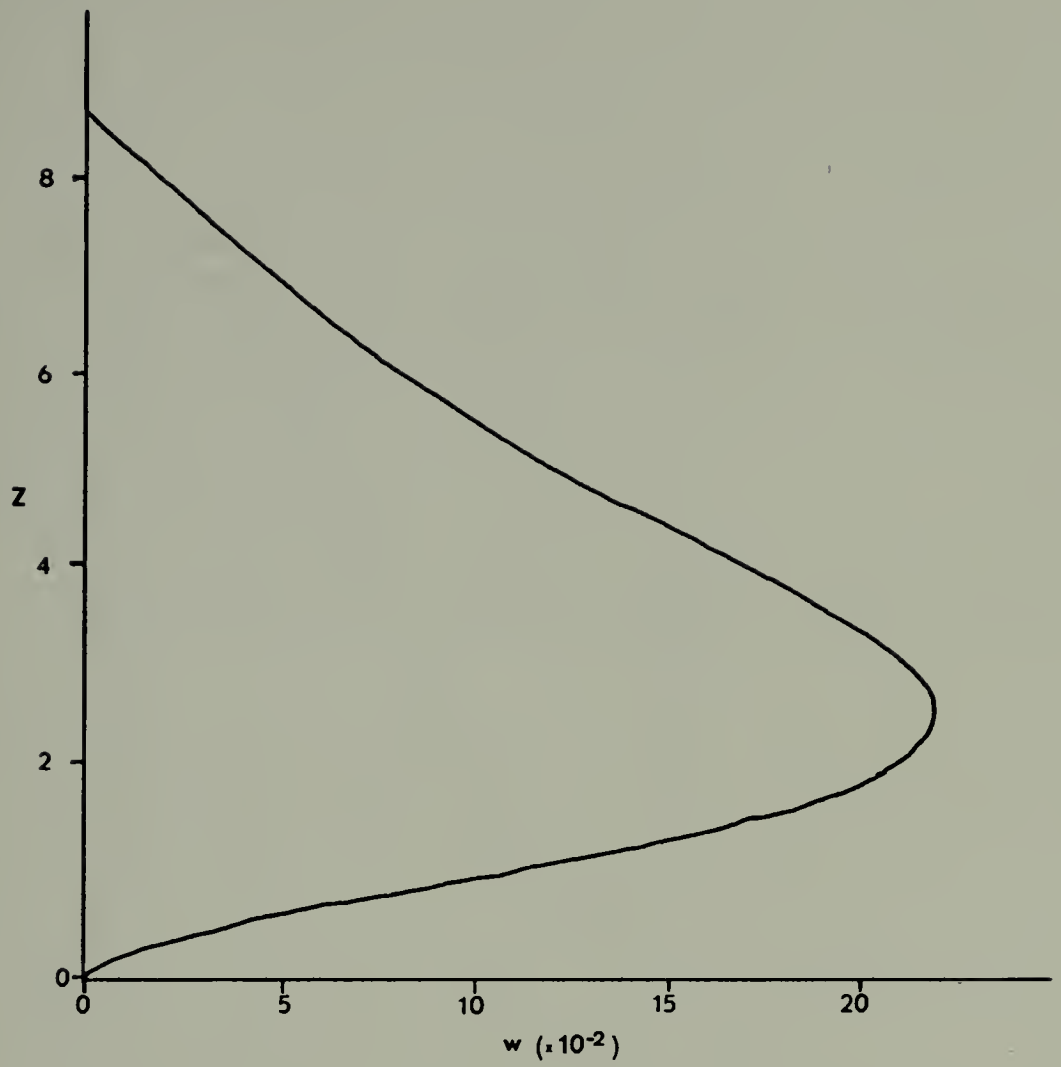

Figure 15. Variation of Vertical Motion with Height at Time = 6 for Model 2, Ro = 1.0.

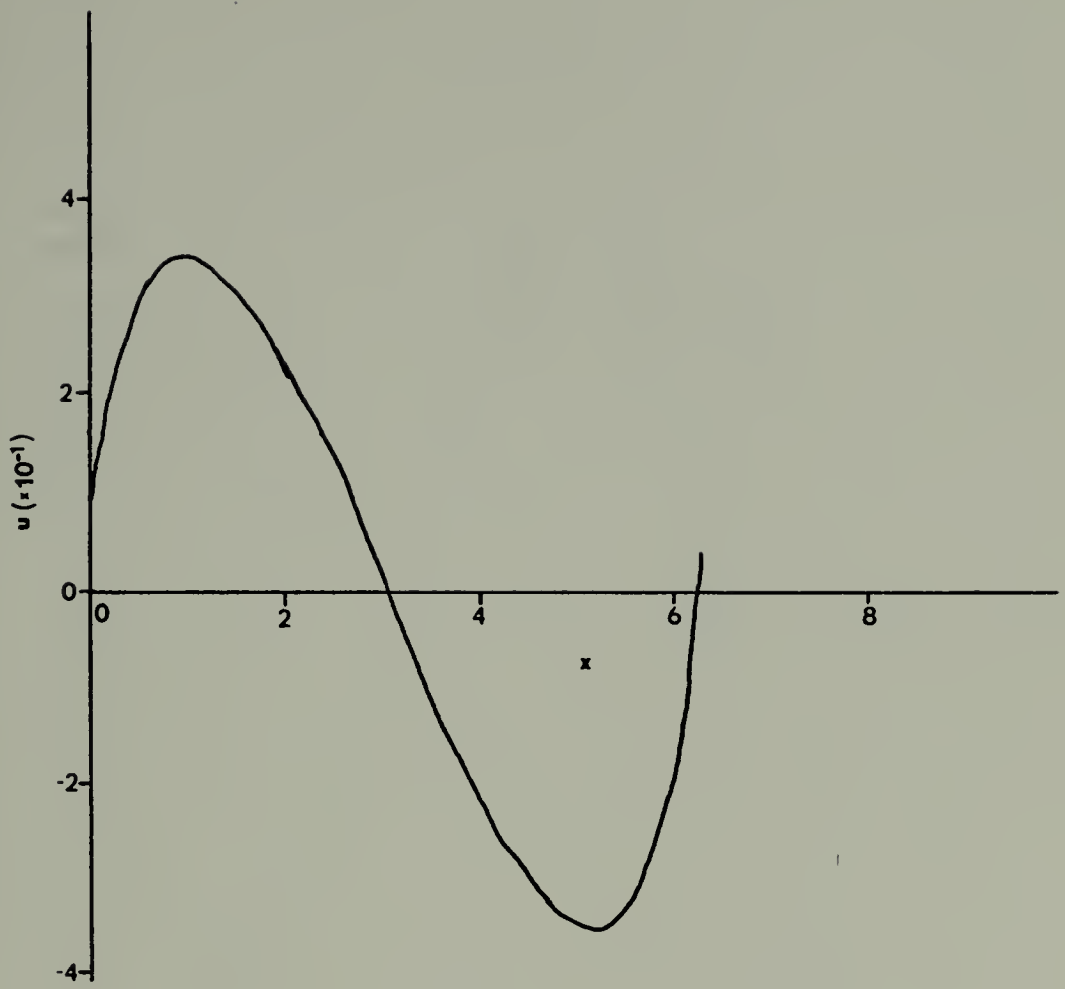

Figure 16. Variation of the u-component of the Wind Field Within the Boundary Layer at z = 1.05 and Time = 6 for Model 3, Ro = 1.0.

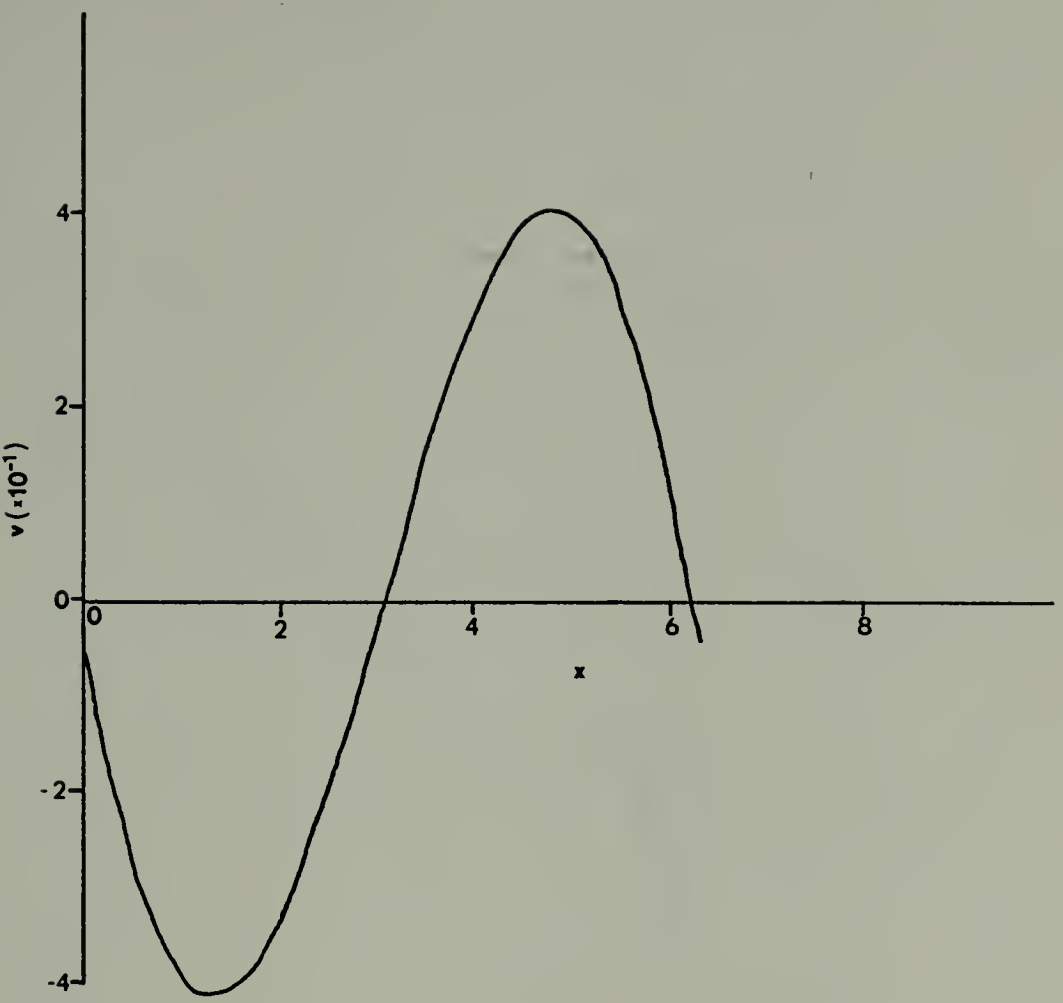

Figure 17. Variation of the v-component of the Wind Field Within the Boundary Layer at z = 1.05 and Time = 6 for Model 3, Ro = 1.0.

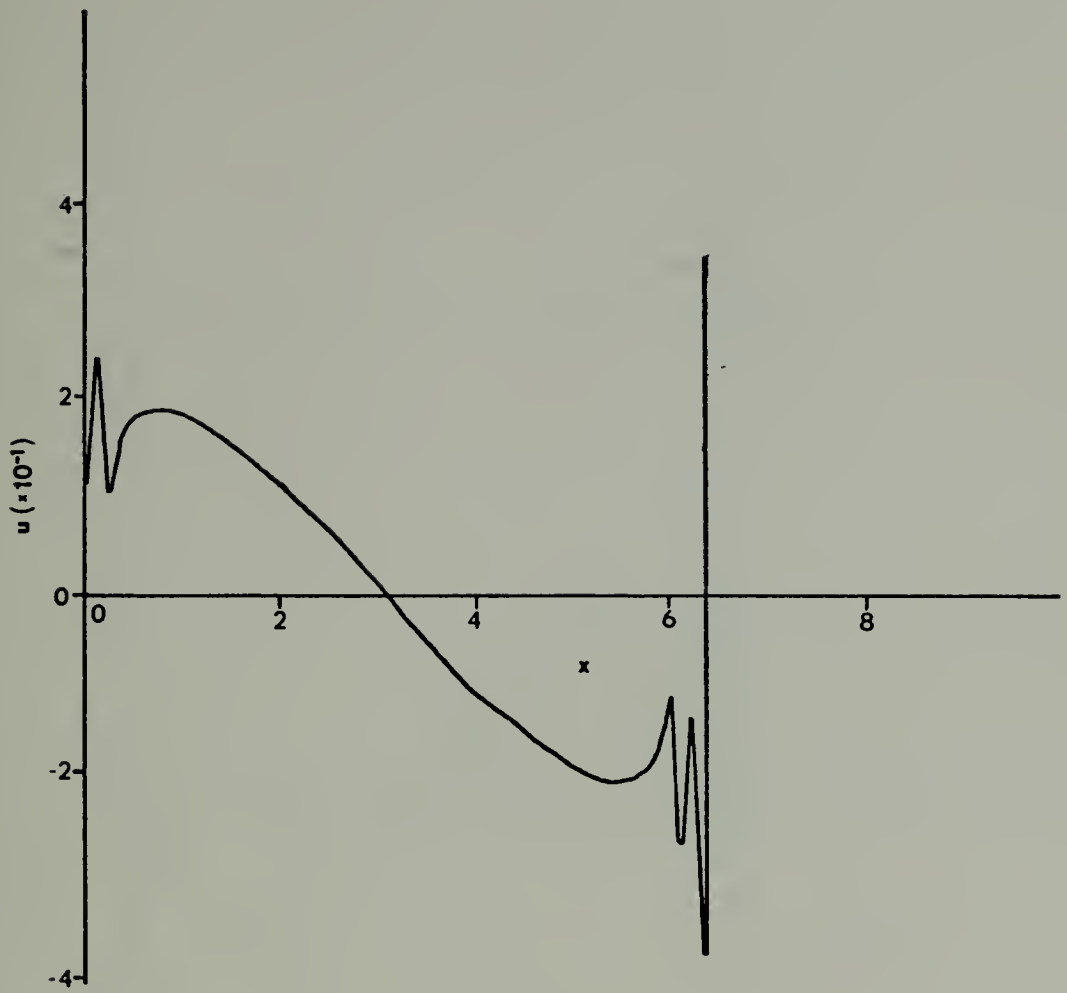

Figure 18. Variation of the u-component of the Wind Field Within the Boundary Layer at z = 1.05 and Time = 6 for Model 3, Ro = 1.5.

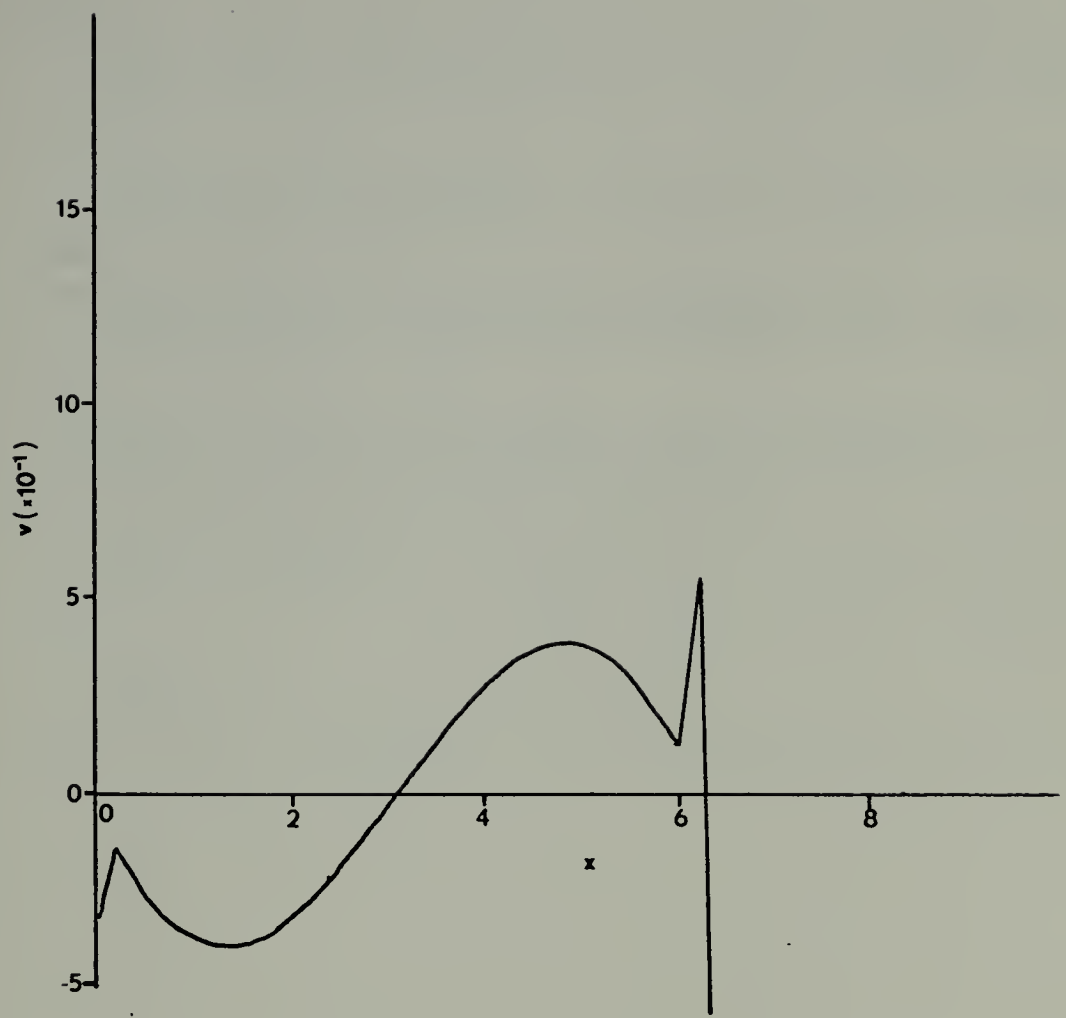

Figure 19. Variation of the v-component of the Wind Field Within the Boundary Layer at z = 1.05 and Time = 6 for Model 3, Ro = 1.5.

LIST OF REFERENCES

1. Arakawa, A., 1966: Computational design for Long-Term Numerical Integrations of the Equations of Atmospheric Motion. J. Computational Phys., vol. 1, pp. 119-143.

2. Benton, G.S., Lipps, F.B. and S.Y. Tuann, 1964: The Structure of the Ekman Layer for Geostrophic Flows with Lateral Shear. Tellus, vol. 16, no. 2, pp. 186-199.

3. Charney, J.G. and A. Eliassen, 1949: A Numerical Method for Predicting the Pertubations of the Middle Latitude Westerlies. Tellus, vol. 1, no. 2, pp. 38-54.

4. Dufort, E.C. and S.P. Frankel, 1953: Stability Conditions in the Numerical Treatment of Parabolic Differential Equations. Math Tables and Other Aids to Computation, vol. 7, p. 135.

5. Holton, J.R., Wallace, J.M. and J.A. Young, 1971: On Boundary Layer Dynamics and the ITCZ. J. Atmos. Sci., vol. 28, no. 2, pp. 275-280.

6. Houghton, D.D. and J.A. Young, 1970: A Note on Inertial Instability. Tellus, vol. 12, no. 5, pp. 581-583.

7. Lorenz, E.N., 1960: Energy and Numerical Weather Prediction. Tellus, vol. 12, pp. 364-373.

INITIAL DISTRIBUTION LIST

		No. Copies
1.	Defense Documentation Center Cameron Station Alexandria, Virginia 22314	2
2.	Library, Code 0212 Naval Postgraduate School Monterey, California 93940	2
3.	Associate Professor Roger T. Williams, Code 51 Department of Meteorology Naval Postgraduate School Monterey, California 93940	10
4.	Lieutenant Commander Carl W. Hoffman, USN U.S. Fleet Weather Central Box 2, COMNAVMARIANAS FPO, San Francisco, California 96630	5
5.	Naval Weather Service Command Washington Navy Yard Washington, D.C. 20390	1
6.	Officer in Charge Naval Weather Research Facility Naval Air Station, Building R-48 Norfolk, Virginia 23511	1
7.	Commanding Officer U.S. Fleet Weather Central COMNAVMARIANAS, Box 12 FPO San Francisco, California 96630	1
8.	Commanding Officer Fleet Weather Central Box 31 FPO New York, New York 09540	1
9.	Commanding Officer Fleet Numerical Weather Central Naval Postgraduate School Monterey, California 93940	1
10.	ARCRL - Research Library L. G. Hanscom Field Attn: Nancy Davis/Stop 29 Bedford, Massachusetts 01730	1

11.	Director, Naval Research Laboratory Attn: Tech. Services Info. Officer Washington, D.C. 20390	1
12.	American Meteorological Society 45 Beacon Street Boston, Massachusetts 02128	1
13.	Department of Meteorology Code 51 Naval Postgraduate School Monterey, California 93940	3
14.	Department of Oceanography Code 58 Naval Postgraduate School Monterey, California 93940	1
15.	Office of Naval Research Department of the Navy Washington, D.C. 20360	1
16.	Commander, Air Weather Service Military Airlift Command U.S. Air Force Scott Air Force Base, Illinois 62226	2
17.	Atmospheric Sciences Library National Oceanographic Atmospheric Administration Silver Springs, Maryland 20910	1
18.	Professor Victor Starr Department of Meteorology M. I. T. Cambridge, Massachusetts 03139	1
19.	Dr. J. Pedlosky Department of Geophysical Sciences University of Chicago Chicago, Illinois 60637	1
20.	Dr. Joanne Simpson Experimental Meteorology Branch National Oceanographic Atmospheric Administration Coral Gables, Florida 33124	1
21.	Dr. V. Jurcec United Nations Development Program Box 982 Cairo, United Arab Republic	1

22. Dr. A. Huss — 1
Department of Meteorology
Hebrew University
Jerusalem, Israel

23. National Center for Atmospheric Research — 1
Box 1470
Boulder, Colorado 80302

24. Dr. T. N. Krishnamurti — 1
Department of Meteorology
Florida State University
Tallahassee, Florida 32306

25. Dr. Fred Shuman — 1
Director
National Meteorological Center
Environmental Science Services Administration
Suitland, Maryland 20390

26. Dr. J. Smagorinsky — 1
Director
Geophysical Fluid Dynamic Laboratory
Princeton University
Princeton, New Jersey 08540

27. Professor N.A. Phillips — 1
54-1422
M. I. T.
Cambridge, Massachusetts 02139

28. Dr. E. N. Lorenz — 1
Department of Meteorology
M. I. T.
Cambridge, Massachusetts 02139

29. Professor J.G. Charney — 1
54-1424
M. I. T.
Cambridge, Massachusetts 02139

30. Professor K. Ooyama — 1
Department of Meteorology
New York University
University Heights
New York, New York 10453

31. Dr. M. G. Wurtele — 1
Department of Meteorology
UCLA
Los Angeles, California 90024

32. Dr. A. Arakawa 1
Department of Meteorology
UCLA
Los Angeles, California 90024

33. Dr. David Houghton 1
Department of Meteorology
University of Winconsin
Madison, Wisconsin 53706

34. Dr. S.K. Kao 1
Department of Meteorology
University of Utah
Salt Lake City, Utah 84112

35. Dr. J. Holton 1
Department of Atmospheric Sciences
University of Washington
Seattle, Washington 98105

36. Dr. P. Gilman 1
National Center for Atmospheric Research
Box 1470
Boulder, Colorado 80302

37. Dr. P. Thompson 1
National Center for Atmospheric Research
Box 1470
Boulder, Colorado 80302

38. Dr. Peter Stone 1
Pierce Hall
Harvard University
Cambridge, Massachusetts 02138

39. Dr. John Young 1
Department of Meteorology
University of Wisconsin
Madison, Wisconsin 53706

40. Dr. George J. Haltiner 1
Chairman, Department of Meteorology
Naval Postgraduate School
Monterey, California 93940

41. Dr. Jerry D. Mahlman
Geophysical Fluid Dynamics Laboratory 1
Princeton University
Princeton, New Jersey 08540

42. Dr. Russell Elsberry — 1
Department of Meteorology
Naval Postgraduate School
Monterey, California 93940

43. Commanding Officer — 1
Pacific Missile Range
Attn: Geophysics Division
Point Mugu, California 93041

44. Dr. Peter J. Gierasch — 1
Geophysical Fluid Dynamics Institute
Florida State University
Tallahassee, Florida 32306

45. Dr. Andrew P. Ingersoll — 1
Division of Geological and Planetary Sciences
California Institute of Technology
Pasadena, California 91109

46. Dr. Robert L. Haney — 1
Department of Meteorology
Naval Postgraduate School
Monterey, California 93940

47. Dr. Ron L. Alberty — 1
Department of Meteorology
Naval Postgraduate School
Monterey, California 93940

48. Dr. W.L. Gates — 1
Department of Meteorology
Naval Postgraduate School
Monterey, California 93940

49. Dr. Richard Alexander — 1
The Rand Corporation
1700 Main Street
Santa Monica, California 90406

50. Commanding Officer — 1
Fleet Weather Central
Box 110
FPO San Francisco, California 96610

51. Dr. G.A. Galt — 1
Department of Oceanography
Naval Postgraduate School
Monterey, California 93940

52. Dr. K.L. Davidson — 1
Department of Meteorology
Naval Postgraduate School
Monterey, California 93940

Security Classification

DOCUMENT CONTROL DATA - R & D

(Security classification of title, body of abstract and indexing annotation must be entered when the overall report is classified)

1. ORIGINATING ACTIVITY (Corporate author)	2a. REPORT SECURITY CLASSIFICATION
Naval Postgraduate School Monterey, California 93940	Unclassified
	2b. GROUP

3. REPORT TITLE

The Relationship Between the Vertical Motion at the Top of the Friction Layer and the Geostrophic Vorticity as a Function of the Rossby Number

4. DESCRIPTIVE NOTES (Type of report and inclusive dates)

Master's Thesis; March 1972

5. AUTHOR(S) (First name, middle initial, last name)

Carl Walter Hoffman

6. REPORT DATE	7a. TOTAL NO. OF PAGES	7b. NO. OF REFS
March 1972	50	7

8a. CONTRACT OR GRANT NO.	9a. ORIGINATOR'S REPORT NUMBER(S)
b. PROJECT NO.	
c.	9b. OTHER REPORT NO(S) (Any other numbers that may be assigned this report)
d.	

10. DISTRIBUTION STATEMENT

Approved for public release; distribution unlimited.

11. SUPPLEMENTARY NOTES	12. SPONSORING MILITARY ACTIVITY
	Naval Postgraduate School Monterey, California 93940

13. ABSTRACT

The relationship between vertical motion at the top of the boundary layer, geostrophic vorticity in the boundary layer and divergence in the boundary layer are examined in this study. The equation of motion and the continuity equation are applied to a homogeneous barotropic atmosphere using a numerical model in this study. The solutions reveal that the boundary layer is stable for very large values of Ro in the case of positive vorticity and becomes unstable at Ro = 1.0 in the case of negative vorticity. A difference in behavior is found between cases of anticyclonic and cyclonic shear. The magnitude of the vertical velocity is greater and the boundary is thicker for anticyclonic than for cyclonic shear systems of equivalent strength.

DD FORM 1 NOV 65 1473 (PAGE 1)

S/N 0101-807-6811

Security Classification

A-31408

14. KEY WORDS	LINK A		LINK B		LINK C	
	ROLE	WT	ROLE	WT	ROLE	WT
Boundary Layer						
Divergence						
Ekman Spiral						
Rossby Number						
Vorticity						

Thesis
H657
c.1

133963

Hoffman
The relationship between the vertical motion at the top of the friction layer and the geostrophic vorticity as a function of the Rossby number.